

# Mechanisms and control technology for roof caving of a roadway in a fold belt in Zhaogu No.2 coal mine, Jiaozuo city, Henan province, China

*To prevent the roof caving of a mining roadway in the No.2[1] coal seam in Zhaogu No.2 coal mine, Jiaozuo city, Henan province, China, we analysed mechanisms of roof caving of the roadway in geological tectonic belt in the coal mine by using comprehensive research methods, such as theoretical analysis, numerical simulation, and field testing. The results demonstrate that: (1) the No.2[1] coal seam contains fault and fold structures and its bidirectional pressure ratio can reach about 3, which affects the shape and extent of the plastic zone in the roadway. (2) Based on the theory of a butterfly-shaped failure zone and numerical simulation, the shape of the plastic zone in the roadway is analysed. It is found that, when the plastic zone in surrounding rock of the roadway presents a butterfly-shaped distribution, large deformation occurs in the roadway when wings of the butterfly-shaped failure zone are just located in roof, floor, and two side walls of the roadway. (3) Due to the significant changes in the plastic zone, anchor bolts are not long enough and anchor cables with limited elongation fail to support the roadway. Therefore, a scheme using long anchor bolts is proposed. The connected long bolts underwent significant elongation and are able to provide a continuous supporting force. This controls the deformation of surrounding rock, thus achieving good supporting effect.*

*Keywords: Fold structure, plastic zone, numerical simulation, mechanism of roof caving, control technology.*

## 1. Introduction

By summarising various accidents in coal mines in recent years, it is found that roof-falls occur most frequently among disasters in many coal mines and lead to a death toll accounting for more than 32% of the total toll in coal mine accidents, also resulting in large property losses [1-5]. Essentially, roof caving of a roadway [6, 7] refers to a certain range of plastic failure in surrounding rock after roadway excavation, accompanied by significant expansion pressure and deformation. If the support structure cannot bear the weight of surrounding rock in the crushed zone under

these conditions, roof caving occurs in the roadway. To maintain the stability of the rock surrounding the roadway, it is necessary to control the development of plastic zones in the rock surrounding the roadway and ensure that it remains stable.

The foundation and key to scientific support design is to master the fracturing mechanisms of the rock surrounding a roadway: the consensus is that deformation and failure of surrounding rock is caused by formation and development of a plastic zone in the surrounding rock, and the range of this plastic zone determines the extent and severity of failure therein. Therefore, to maintain the stability of surrounding rocks of roadways, it is necessary to control the development of the plastic zone therein and ensure its stability. As for research on the boundary of the plastic zone in surrounding rock, the plastic zone is generally thought to have several shapes (circular, elliptical, arcuate (formed by natural caving), irregular blocky forms, and butterfly shaped as analysed here).

Nowadays, commonly used theories of plastic zone include Finner and Castellner's theory of a circular plastic zone [11-13], support theory for loose zones in surrounding rock proposed by Prof. Dong Fangting [14], a theory of arching formed by natural caving, a theory of axial variation proposed by Professor Yu Xuefu, and a theory of zonal disintegration distribution in surrounding rock [15]. These theories fail to explain the extent of the plastic zone in rock surrounding a roadway under high deviatoric stress. The theory of butterfly-shaped failure zone proposed by Professor Ma Nianjie et al. suggested that the plastic zone is distributed in a butterfly shape under bidirectional unequal pressures. Moreover, they proposed a theoretical formula describing the butterfly-shaped failure zone [16, 17] and introduced a component of deviatoric stress to analyse the aforementioned butterfly-shaped failure zone.

At present, the primary mineable coal seam in Zhaogu No.2 coal mine is about 700 m deep with high ground pressure with extremely thick alluvium and thin bedrock. Developed fractures and unstable roof and floor of the coal seam mean that roof caving frequently occurs in local areas, so that the roadway is needed to be renovated many times, with attendant implications for safety and productivity. For a long

Mr. Gao Xu, School of Energy and Mining Engineering, China University of Mining & Technology, Beijing 10083, China.

time, deformation and failure of surrounding rock have been reduced by constantly increasing the strength of anchor bolt and cable and the initial anchor force. For example, measures, such as greatly increasing number and diameter of anchor cables are taken. Moreover, the length of anchor cables is also extended and the length of anchor cables in a roadway with span of 5 m has been 8 to 10 m: however, such a high-strength support does not achieve ideal control effects on roof caving of the roadway.

Based on the theory of F, we discussed and analysed a reasonable support shape by analysing the shapes of actual plastic zones in a geological tectonic belt in a coal roadway of Zhaogu No.2 coal mine.

## 2. Theory of butterfly-shaped failure

### 2.1 ELASTO-PLASTIC STRESS FIELD IN SURROUNDING ROCK OF A CIRCULAR ROADWAY BUILT IN A HOMOGENEOUS ROCK MASS

For the convenience of theoretical analysis, the surrounding rock of the roadway is first assumed to be homogeneous, continuous, isotropic, and linearly elastic. Furthermore, creep and viscosity effects are deemed negligible and the surrounding rock is unaffected by factors, such as geological structure, water and rock structures, so a uniformly distributed load is considered to generate the stress field. In situ rock stresses in the horizontal and vertical directions in a cross-section of the roadway are unchanged along the lengthwise direction of the roadway. The cross-section of the roadway is circular and the properties of surrounding rock are consistent for a roadway with infinite length (plane strain conditions therefore applied).

When the conditions of burial depth are met and burial depth is greater than or equal to 20 times the radius of the roadway, the error with the original problem is no more than 5% if the self-weight of rock in the zone of influence (five times the radius of the roadway) of the roadway is ignored.

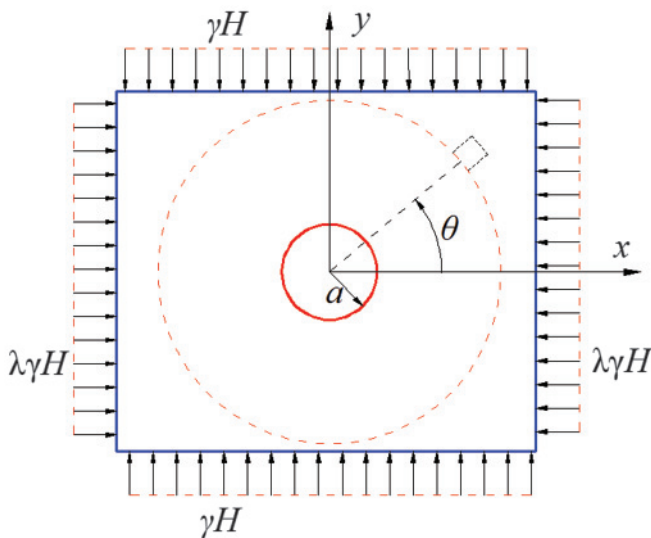


Fig.1 Mechanical model of a circular hole

Therefore, in situ stress in the horizontal direction can be simplified to a uniform distribution. In this way, the actual roadway model can be simplified to a plane strain problem with a circular hole, for which loads and structures are axisymmetric in elasto-plastic mechanics (Fig.1).

In accordance with the established mechanical model, for the feasibility of theoretical calculation, it is assumed that the stress field is geostatic. By using the solution to two-dimensional stress distribution around the circular hole in an elastic plane, the stress solution at any point in the rock surrounding a circular roadway in a polar coordinate system can be obtained:

$$\begin{cases} \sigma_r = \frac{\gamma H}{2} \left[ (1+\lambda) \left( 1 - \frac{a^2}{R_\theta^2} \right) + (\lambda-1) \left( 1 - 4\frac{a^2}{R_\theta^2} + 3\frac{a^4}{R_\theta^4} \right) \cos 2\theta \right] \\ \sigma_\theta = \frac{\gamma H}{2} \left[ (1+\lambda) \left( 1 + \frac{a^2}{R_\theta^2} \right) - (\lambda-1) \left( 1 + 3\frac{a^4}{R_\theta^4} \right) \cos 2\theta \right] \\ \tau_{r\theta} = \frac{\gamma H}{2} \left[ (\lambda-1) \left( 1 + 2\frac{a^2}{R_\theta^2} - 3\frac{a^4}{R_\theta^4} \right) \sin 2\theta \right] \end{cases} \quad (1)$$

where,  $\sigma_r$ ,  $\sigma_\theta$  and  $\tau_{r\theta}$  represent the radial stress, circumferential stress, and shear stress at any point, respectively;  $\gamma$ ,  $H$ ,  $\lambda$ , and  $a$  separately indicate the unit weight of rock, the burial depth of the roadway, the lateral pressure coefficient, and the radius of the circular roadway;  $R_\theta$ ,  $\theta$  denote the polar coordinates of any point.

To obtain principal stress at any point in the surrounding rock of the circular roadway, the stress formula in the polar coordinate system should be transformed into that in a rectangular coordinate system through use of the following formula:

$$\begin{cases} \sigma_x = \frac{\sigma_r + \sigma_\theta}{2} + \frac{\sigma_r - \sigma_\theta}{2} \cos 2\theta - \tau_{r\theta} \sin 2\theta \\ \sigma_y = \frac{\sigma_r + \sigma_\theta}{2} - \frac{\sigma_r - \sigma_\theta}{2} \cos 2\theta + \tau_{r\theta} \sin 2\theta \\ \tau_{xy} = \frac{\sigma_r - \sigma_\theta}{2} \sin 2\theta + \tau_{r\theta} \cos 2\theta \end{cases} \quad \dots (2)$$

The principal stress in elastic mechanics is given by:

$$\begin{cases} \sigma_1 = \frac{\sigma_x + \sigma_y}{2} + \frac{1}{2} \sqrt{(\sigma_x - \sigma_y)^2 + 4\tau_{xy}^2} \\ \sigma_3 = \frac{\sigma_x + \sigma_y}{2} - \frac{1}{2} \sqrt{(\sigma_x - \sigma_y)^2 + 4\tau_{xy}^2} \end{cases} \quad \dots (3)$$

After substituting Formula (1.1) into Formula (1.2) and then Formula (1.3), the principal stress at any point in the rock surrounding a circular roadway represented by polar coordinates is given by:

$$\begin{cases} \sigma_1 = \frac{\sigma_r + \sigma_\theta}{2} + \frac{1}{2} \sqrt{(\sigma_r - \sigma_\theta)^2 + 4\tau_{r\theta}^2} \\ \sigma_3 = \frac{\sigma_r + \sigma_\theta}{2} - \frac{1}{2} \sqrt{(\sigma_r - \sigma_\theta)^2 + 4\tau_{r\theta}^2} \end{cases} \quad \dots (4)$$

The traditional theory for the failure of surrounding rock of a roadway considers that it is the pressure on surrounding

rock that plays a key role in the failure thereof. In the support design, pressure applied to surrounding rock is a key influence factor. This idea has a certain guiding significance for support design in a roadway at shallow burial depth, however, for deep roadways disturbed by mining, conventional theories of surrounding rock failure are inapplicable. Plastic mechanics of rock and soil show that plastic failure of surrounding rock of the roadway and its evolution are mainly determined by deviatoric stress. Surrounding rock stress is the superposition of *in situ* rock stress and deviatoric stress, and is significant with regard to its influence on the plastic failure of rock [17].

The stress state at a point is bound to show three principal stress directions. When stress state of a point is represented by principal stresses, stress can be expressed as follows:

$$\sigma_i = \sigma_m + S_i \quad \dots (5)$$

where,  $s_i$  and  $\sigma_m$  indicate the principal deviatoric stress and average stress, respectively.

$$\sigma_m = \frac{\sigma_1 + \sigma_2 + \sigma_3}{3} \quad \dots (6)$$

When studying stresses in the rock surrounding a roadway, plane stress conditions (according to formula (5) and (6)), the principal deviatoric stress  $s_i$  is given by:

$$\begin{cases} s_1 = \frac{2\sigma_1 - \sigma_3}{3} \\ s_3 = \frac{2\sigma_3 - \sigma_1}{3} \end{cases} \quad \dots (7)$$

By substituting formula (1.4) into formula (1.7), the following formula can be obtained:

$$\begin{cases} s_1 = \frac{\sigma_r + \sigma_\theta}{6} + \frac{\sqrt{(\sigma_r - \sigma_\theta)^2 + 4\tau_{r\theta}^2}}{2} \\ s_3 = \frac{\sigma_r + \sigma_\theta}{6} - \frac{\sqrt{(\sigma_r - \sigma_\theta)^2 + 4\tau_{r\theta}^2}}{2} \end{cases} \quad \dots (8)$$

## 2.2 STRENGTH CRITERION OF SURROUNDING ROCK

The Mohr-Coulomb strength criterion is the most widely used criterion at present. This theory considers that the failure at any point in the rock surrounding a roadway is related to the maximum and minimum principal stress applied thereat. When the pressure is low, ultimate equilibrium conditions of surrounding rock mass can be expressed by the linear Mohr envelope, that is, when a rock mass reaches its elastic limit and is under plastic equilibrium conditions, its stress state satisfies the following formula:

$$\tau = C + \sigma \tan \varphi \quad \dots (9)$$

where,  $\tau$ ,  $C$ ,  $\sigma$  and  $\varphi$  indicate the tangential stress (MPa), cohesion (MPa), normal stress (MPa), and angle of internal friction ( $^\circ$ ) of a point in the surrounding rock, respectively.

After determining the principal stresses, the Mohr-Coulomb strength criterion represented by ultimate principal

stresses  $\sigma_1$  and  $\sigma_3$ , is as follows:

$$\sigma_1 = 2C \frac{\cos \varphi}{1 - \sin \varphi} + \frac{1 + \sin \varphi}{1 - \sin \varphi} \sigma_3 \quad \dots (10)$$

where,  $\sigma_1 - 2C \frac{\cos \varphi}{1 - \sin \varphi} - \frac{1 + \sin \varphi}{1 - \sin \varphi} \sigma_3 = 0$  indicates that the rock surrounding the roadway is at the critical point of elasticity and plasticity. If,  $\sigma_1 - 2C \frac{\cos \varphi}{1 - \sin \varphi} - \frac{1 + \sin \varphi}{1 - \sin \varphi} \sigma_3 > 0$ , then the surrounding rock enters the plastic state.

By transforming formula (3 to 10), the following formula can be obtained:

$$(\sigma_1 - \sigma_3) - (\sigma_1 + \sigma_3) \sin \varphi = 2C \cos \varphi \quad \dots (11)$$

## 2.3 DETERMINATION OF BOUNDARY OF PLASTIC ZONE IN SURROUNDING ROCK OF THE ROADWAY IN A NON-UNIFORM STRESS FIELD

To facilitate calculation of boundary of plastic zone in surrounding rock of a roadway in a non-uniform stress field, the following formula can be obtained by transforming formula (11).

$$s_1 - s_2 - (\sigma_1 + \sigma_3) \sin \varphi = 2C \cos \varphi \quad \dots (12)$$

$$2\gamma H(1 - \lambda) \sin \varphi \cos 2\theta \frac{a^2}{r^2} = 2C \cos \varphi + \gamma H(1 + \lambda) \sin \varphi - (s_1 - s_3) \quad \dots (13)$$

Therefore, through formula (13), the radius of plastic zone in the rock surrounding a circular roadway in a non-uniform stress field can be obtained [18]:

$$R_\theta = \sqrt{\frac{2a^2 \gamma H \sin \varphi \cos 2\theta (1 - \lambda)}{2C \cos \varphi + \gamma H(1 + \lambda) \sin \varphi - (s_1 - s_3)}} \quad \dots (14)$$

Therefore, boundary of the plastic zone in the rock surrounding a roadway in a non-uniform stress field can be obtained by combining formula (14) with formula (1) and (8). It can be seen that factors including burial depth  $H$  of the roadway, unit weight  $\gamma$  of surrounding rock, lateral pressure coefficient  $\lambda$ , radius  $a$  of the roadway, cohesion  $C$ , and angle  $\varphi$  of internal friction of surrounding rock influence the plastic zone. Given the above parameters, the boundary of the plastic zone can be calculated.

## 2.4 DIRECTIVITY OF BUTTERFLY WINGS OF BUTTERFLY-SHAPED FAILURE ZONE IN THE ROCK SURROUNDING A ROADWAY

When the shape and size of butterfly-shaped failure zone are known, it is the orientation of the butterfly wings that plays a decisive role in roadway stability. Deformation and failure of the rock surrounding a roadway mainly result from plastic zones therein. When the wings of the butterfly-shaped failure zone are above the roof, the roof is plastically fractured to a large depth and has the lowest stability. Therefore, directivity of butterfly wings of butterfly-shaped failure zones in surrounding rock is key to understanding mechanisms of roof caving. For convenience of analysis, the angle between the axis of symmetry of butterfly wings and a line perpendicular to the interface of a layered rock mass is defined as the deviation angle ( $\beta$ ) of the butterfly wings.

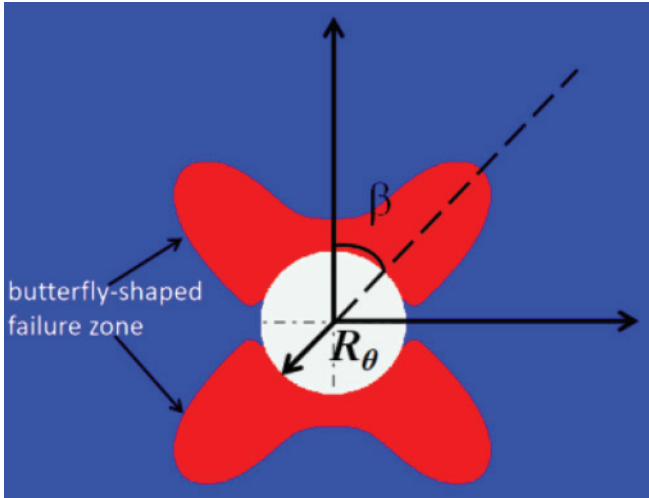


Fig.2 Schematic characterisation of main dimensions of plastic zone in the rock surrounding a roadway

The direction of principal stress corresponds to direction of butterfly wings of the butterfly-shaped failure zone. Fig.3 shows the relationship between the orientation of butterfly wings and direction of principal stress. It can be seen that when the maximum principal stress is in the horizontal direction, the butterfly wings of the plastic zone tilt at approximately 45° and extend towards roof and floor, so the deviation angle ( $\beta$ ) of the butterfly wings is 45°. With the rotation of the direction of the maximum principal stress, the direction of the butterfly wings also deflects by the same angle. When the direction of the maximum principal stress is at 45° to the vertical, the butterfly-shaped failure zone is located directly above the roof ( $\beta = 0^\circ$ ). Such orientation and shape of the butterfly-shaped failure zone are most unfavourable for the stability of the roadway roof; however, in the stress field around a roadway with a butterfly-shaped failure zone and high deviatoric stress, the principal stress is generally not in the horizontal or vertical directions, so the butterfly wings of the plastic zone point towards the roof.

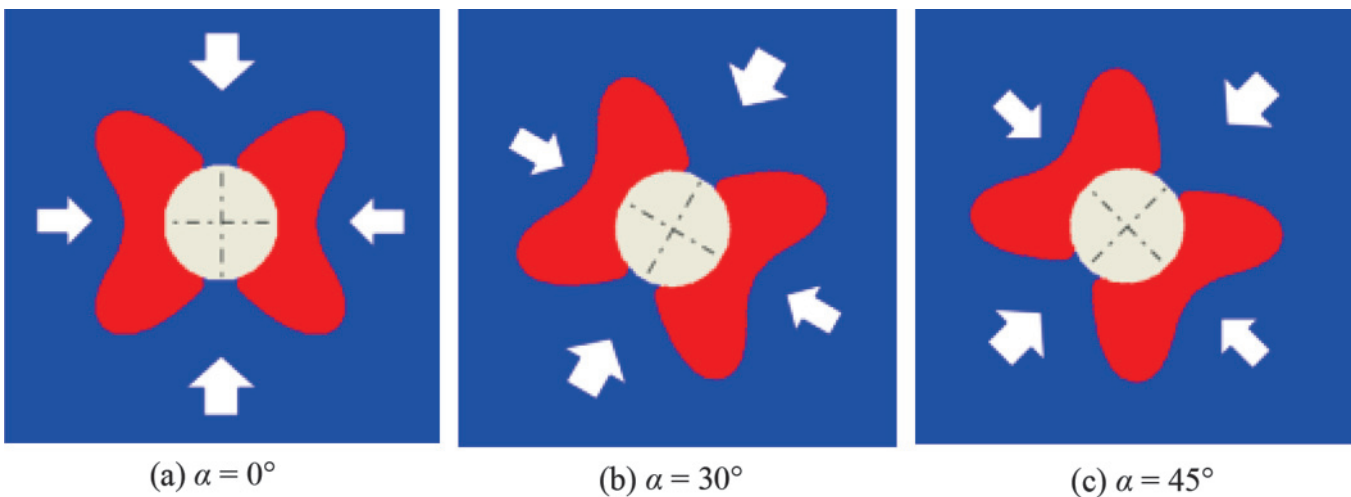


Fig.3 Relationship between shape of butterfly-shaped failure zone and the direction of the principal stress

### 3 Engineering background and detection of rock structures in the roof

#### 3.1 ENGINEERING BACKGROUND

The chosen mine was designed to have production of 2.4 Mt/a and was developed by building vertical shafts. The No.2[1] coal seam was the primary mineable seam. As shown in Fig.1, the roof was mainly composed of sandy mudstone and fine-grained sandstone. The immediate roof was generally 1~6.5 m thick and average thickness was 5.3 m, while the main roof had a thickness of 0.94~19.85 m and average thickness of 7.46 m consisting of coarse, medium, and fine-grained sandstones: mudstone, and sandy mudstone were mainly found in the floor. The burial depth was about 705 m and dip of the coal seam varied from 0° to 11°. Roadways were arranged in the zonal layout in the mine and fully-mechanised mining was adopted. Moreover, the roof was controlled by using a backwards full-caving method. Owing to fractures having been developed in the coal seam and roof and floor were unstable, localised roof caving was frequent. The rock mass in some zones showed characteristic folding, and the horizontal stress in fold belts increased, making roadway failure more severe.

#### 3.2 BOREHOLE IMAGING OF THE ROOF

Based on the research objective and specific situation in the field, to elucidate the characteristics of each strata structure in the roadway roof, the strata structure has to be detected first. The roof in the roadway stabilised after being subjected to mining-induced disturbance in the fold belt (as observed through borehole imaging). The distributions of measurement points are shown in Fig.4 and observation results are summarised in Tables 1 to 3.

By analysing these three groups of data, it can be seen that overlying strata in the roof of the roadway in Zhaogu No.2 coal mine basically comprised sandy mudstone, siltstone, and fine-grained sandstone. Crushing mainly occurred within 1.5 m from the roof and bedding separation was common.

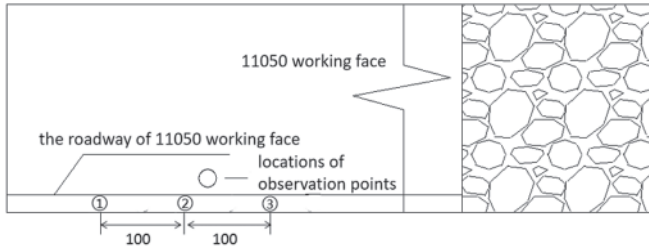


Fig.4 Locations of observation points

### 3.3 STRESS STATE IN THE ROCK SURROUNDING A ROADWAY IN THE FOLD BELT

No.2[1] coal seam in Zhaogu No.2 coal mine contains fault and fold structures with different degrees of development: these deform and damage rock surrounding the roadway in the tectonic zone, so it is difficult to support the workings. Chen et al. [18] evaluated the stress field in the fold tectonic zone and Zheng Wenhai [17] studied the method of numerical simulation for distribution *in situ* stress. Based on this, a model was established through numerical simulation based on burial depth and rock mechanics parameters of the fold belt in the 11050 working face (Fig.5). The model was defined as a material model and gravitational load was applied to the upper surface of the model to simulate the burial depth. Boundary conditions are set as follows: the upper boundary is free, while the lower boundary, as well as boundaries to the front and rear, are constrained. A certain displacement and strain rate were applied to both left and right sides of the model, so

that each stratum is shortened in the horizontal direction and hard, competent strata bend in the longitudinal direction to form a fold. In the calculation, fold amplitude (represented by the dip angle of wings which in this study is defined as the dip angle of the line connecting the highest point of anticline and the lowest point of syncline) was controlled in accordance with number of iteration times. Firstly, a 0.001 m/step displacement rate of change was applied and saved after 10,000 calculation steps, followed by calculation of a further 10,000 steps. In this way, a total of 30,000 steps were calculated to complete the simulation. By extracting principal stresses around the fold structure in the model, a stress concentration was found in the fold structure and the

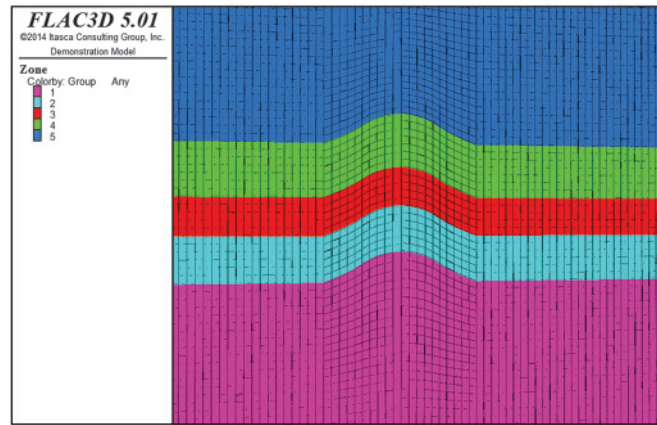


Fig.5 Model of the fold belt

TABLE 1 COLUMN AND TYPICAL CROSS-SECTIONS OF A BOREHOLE IN ROOF AT OBSERVATION POINT 1 IN THE ROADWAY OF THE 11050 WORKING FACE

Description	Column	Layer thickness (m)	Cumulative depth (m)	Remark
Fine grained sandstone		5.4	10	The fine grained sandstone is gray and mainly shows quartz, star-shaped minerals and mica fragments. It has obvious horizontal bedding and good stability.
Siltstone		0.6	4.6	
Sandy mudstone		4	4	It is gray and mainly contains quartz, star-shaped minerals and mica fragments. It shows obvious horizontal bedding and good stability.

	Crushing at 0.97 m		Bedding separation at 2.31 m
	Crushing at 2.37 m		Sandy mudstone

TABLE 2 COLUMN AND TYPICAL CROSS-SECTIONS OF A BOREHOLE IN ROOF AT OBSERVATION POINT 2 IN THE INTAKE AIRWAY OF THE 1050 WORKING FACE

Description	Column	Layer thickness (m)	Cumulative depth (m)	Remark
Fine grained sandstone		2.5	10	The fine grained sandstone is gray and mainly shows quartz, star-shaped minerals and mica fragments. It has obvious horizontal bedding and good stability.
Siltstone		4.9	7.5	
Sandy mudstone		2.6	2.6	It is gray and mainly contains quartz, star-shaped minerals and mica fragments. It shows obvious horizontal bedding and good stability.

Bedding separation at 0.74 m	Sandy mudstone
Bedding separation at 2.38 m	Bedding separation at 4.32 m

TABLE 3 COLUMN AND TYPICAL CROSS-SECTIONS OF A BOREHOLE IN ROOF IN OBSERVATION POINT 3 IN THE INTAKE AIRWAY OF THE 11050 WORKING FACE

Description	Column	Layer thickness (m)	Cumulative depth (m)	Remark
Fine grained sandstone		3.8	10	The fine grained sandstone is gray and mainly shows quartz, star-shaped minerals and mica fragments. It has obvious horizontal bedding and good stability.
Siltstone		3.3	6.2	
Sandy mudstone		2.9	2.9	It is gray and mainly contains quartz, star-shaped minerals and mica fragments. It shows obvious horizontal bedding and good stability.

Crushing at 0.47 m	Crushing at 0.65 m
Bedding separation at 1.92 m	Bedding separation at 6.07 m

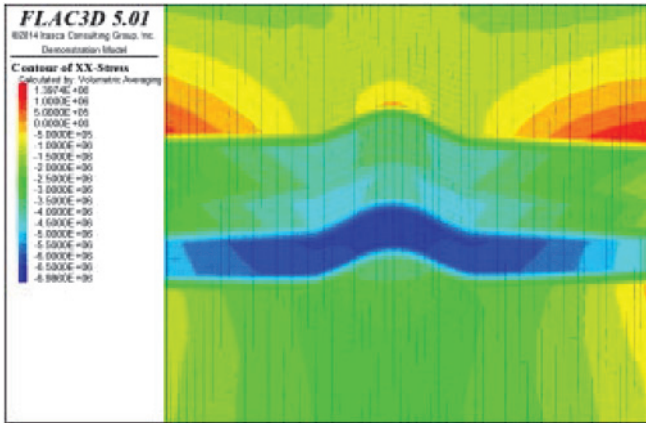


Fig.6 Cloud picture of horizontal stress

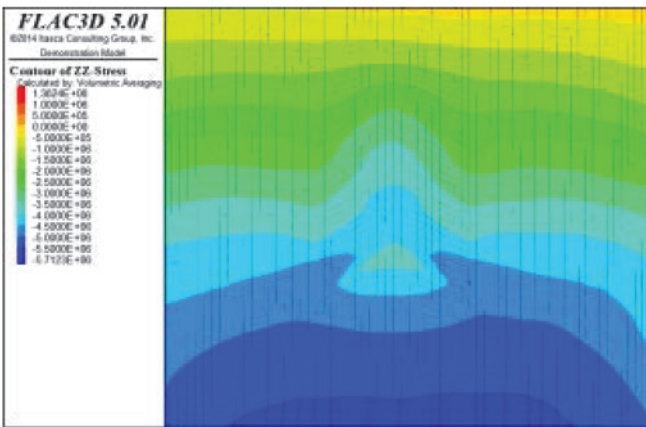


Fig.7 Cloud picture of vertical stress

ratio of the maximum principal stress to the minimum principal stress was about 3. Cloud pictures of horizontal and vertical stresses are displayed in Figs.6 and 7.

According to results of numerical simulation, if a rock mass contains fewer fractures at small-scale, layered strata do not tend to bend or deform (this can be regarded as a normal stress zone). The rock mass in this zone can be approximately considered as being in an isobaric stress field. If stress is highly concentrated on the axial surface of the fold, especially when the horizontal stress reaches about three times that of normal horizontal stress so that the bidirectional pressure ratio of stress field in this zone approaches 3 and the direction of principal stress deflects to some extent, then this zone is a high horizontal stress concentration zone. A transition zone is found between the normal stress zone and the high horizontal stress concentration zone and shows a lower degree of stress concentration. Moreover, the bidirectional pressure ratio ranges from 1 to 3 (Fig.8).

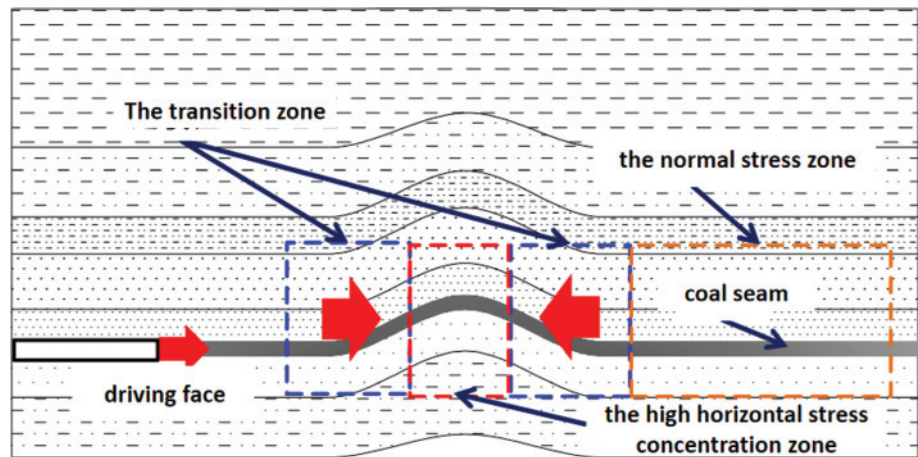


Fig.8 Schematic diagram showing characteristics of the stress environment around the fold

### 3.4 SIMULATION OF THE INFLUENCES OF GEOLOGICAL STRUCTURE ON THE ROADWAY

The transport roadway in the 11050 working face in Zhaogu No.2 coal mine was taken as a research object, in which some sections are located in the fold. Therefore, a special stress environment (different lateral pressure coefficients) of the fold affects the plastic failure of surrounding rock in the coal roadway. Under the same geological conditions, the distribution of plastic zones in the rock surrounding the roadway is obtained when the lateral pressure coefficients are 1, 2, and 3 (Figs. 9 to 11).

Fig.9 shows the distribution of plastic zones when the coal roadway is unaffected by geological structures and mining ( $\lambda=1$ ): the plastic zone is distributed uniformly in the rock surrounding the roadway, the range of surrounding rock failure is small with a maximum failure depth of 0.5 m, indicating favourable overall stability of the roadway. Under these conditions, the roof of the roadway is not prone to caving, so support with general anchor bolts can meet engineering demands.

Fig.10 shows the distribution of plastic zones in the surrounding rock when the coal roadway lies in the wings of the fold structure (transition zone,  $\lambda = 2$ ). It can be observed that, under the influences of high lateral pressure in wings of the fold structure, the shape of the plastic zone changes: because the maximum principal stress deviates leftwards by  $45^\circ$  from the vertical, rock in left side of the floor, lower part of the left side wall, right side of the roof, and upper part of the right side wall is severely damaged and the maximum failure range of plastic zone is 1.5 m. The plastic zone in the other parts around the roadway is within a 0.5 m depth range and the roadway remains relatively good in terms of overall stability. Under these conditions, the roof of the roadway is easy to control and unlikely to cave.

Fig.11 shows the distribution of the plastic zone in surrounding rock when the coal roadway is located in the zone near the axial surface of the fold (high stress

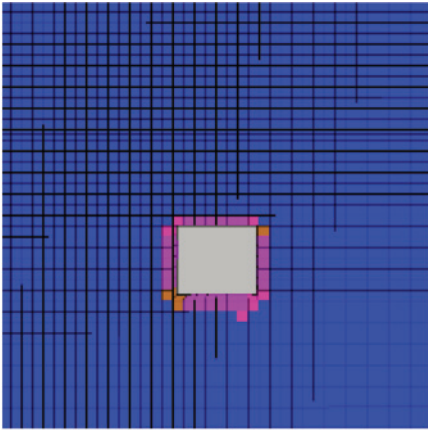


Fig.9 Lateral pressure coefficient  $\lambda = 1$

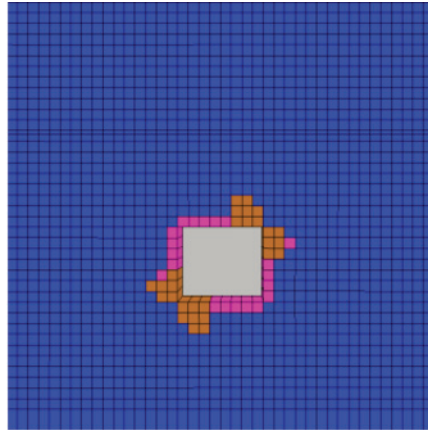


Fig.10 Lateral pressure coefficient  $\lambda = 2$

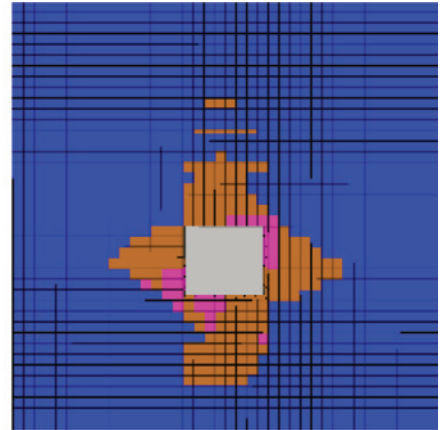


Fig.11 Lateral pressure coefficient  $\lambda = 3$

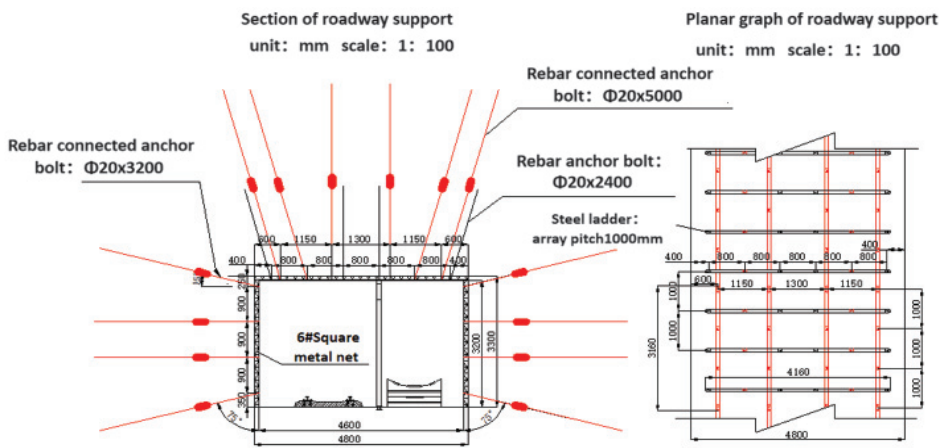


Fig.12 Schematic diagram of flat section in the scheme of combined support with long anchor bolts

roadway is 6.0 m and interlayer failure also occurs in weak intercalated layers between stable strata above the roof. In addition, the failure ranges of two side walls of the roadway are equivalent and the maximum failure range is 6.0 m. Under these conditions, it is difficult to maintain the roadway, so the length of supporting body should exceed the maximum failure depth of rock in the roof. When the roadway is not appropriately supported, the roof is liable to cave.

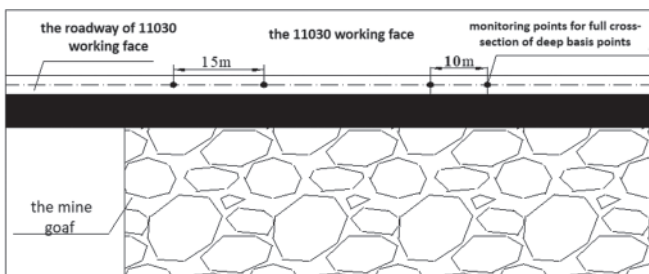


Fig.13 Location of monitoring stations for displacement of deep basis points

concentration zone,  $\lambda = 3$ ): in the high stress concentration zone near the axial surface of the fold, the plastic zone is distributed in a butterfly shape. When the maximum principal stress deviates by  $45^\circ$  from the vertical direction, the butterfly wings are just located in the roof, floor, and two side walls of the roadway. In this case, rock in the roof, floor, and two side walls of the roadway are severely damaged, so the roadway exhibits low overall stability. Due to lithologic differences between the roof and floor, plastic failure in the floor of the roadway extends the most and the maximum failure depth reaches 4 m. The maximum failure depth of roof of the

#### 4. Control countermeasures for roof caving of the roadway in the tectonic zone

The bidirectional pressure ratio (the ratio of the maximum principal stress to the minimum principal stress) in the working face tends to 3: under these conditions, the plastic zone appears as a butterfly. Meanwhile, when the maximum principal stress deviates by  $45^\circ$  from the vertical direction, the wings of the butterfly-shaped failure zone lie in the roof, floor, and two side walls of the roadway. In this case, rock in the roof, floor, and two side walls of the roadway is severely damaged, resulting in low overall stability. The failure depth of the roof of the roadway is 3 m and a small range of interlayer failures occur due to the presence of weak intercalated layers in the roof of the roadway.

Under such conditions, a large depth range of butterfly shaped failure in roof of the roadway causes severe deformation, thus resulting in significant roof deformation. In terms of the supporting body, in addition to ensuring sufficient strength, it also should have sufficient elongation for a roof subject to large deformation. Although it meets the requirements for strength, combined anchor bolt and cable supports are inapplicable as their elongation is not suitable

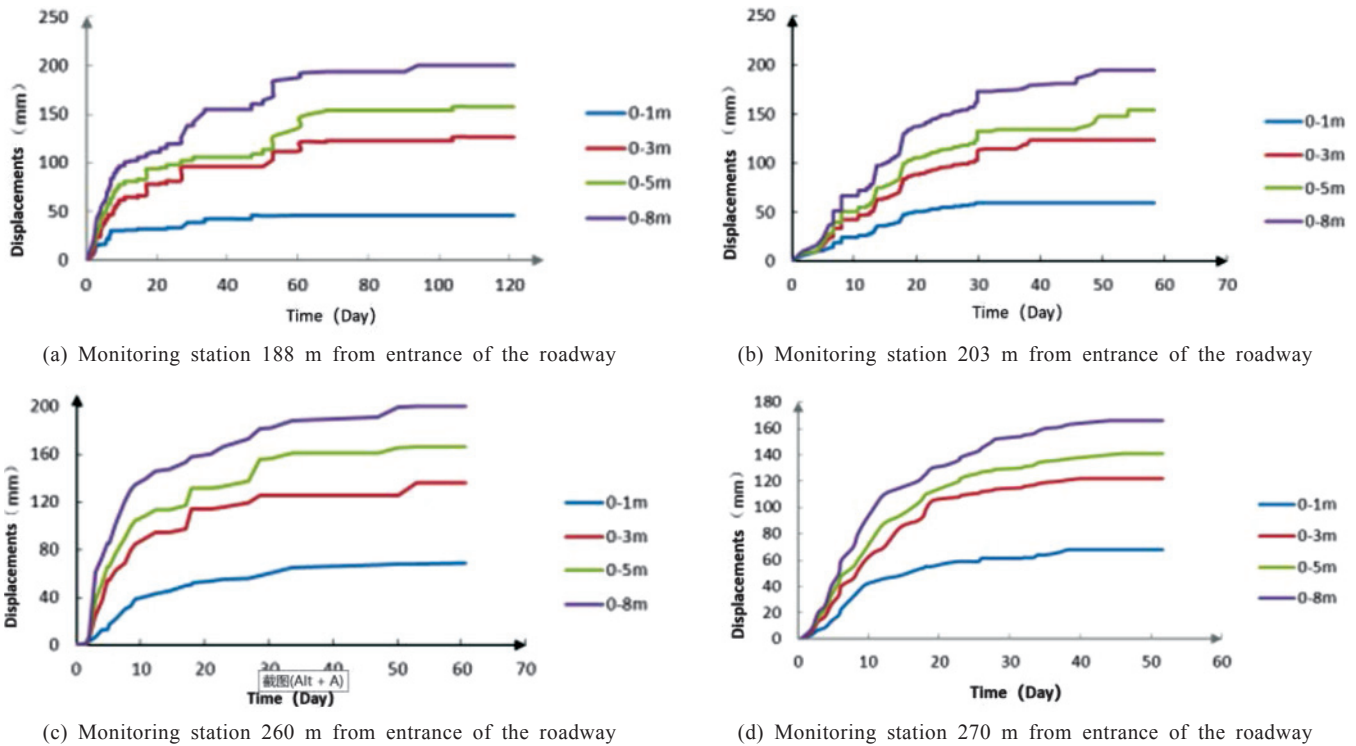


Fig.14 Curves of roof deformation at different locations of the roadway under test

for the large deformation expected in such a roadway roof. In view of the risk of roof caving while mining the roadway in Zhaogu No.2 coal mine, long anchor bolts cannot be installed due to the limited cross-sectional dimensions of the roadway. Therefore, by studying control technologies, the scheme of combined support with connected long bolts [19] was proposed.

Tests were conducted to draw the connected long bolts with dimension of  $\Phi 20 \times 5000$  mm by using a bolt drawing machine with a wide range and results were recorded every 10 to 20 mm. Test results show that at an extension of 40 mm, the drawing force was 22 kN. After that, with increasing extension, the drawing force increased in a quasi-linear fashion. As the extension exceeded about 90 mm, the drawing force changed slightly. In the range of 165 to 180 kN, due to the limited range of the bolt drawing machine, the connected long bolts were not fractured. Moreover, within 430 mm extension, the drawing force was stable. The weight of broken body per metre of roadway roof is about 360 kN according to the numerical simulation. On this basis and by referring to design formula for support parameters (Chang *et al.* [20]), the support parameters of the roadway were designed as described below.

Ordinary rebar anchor bolts ( $\phi 20 \times 2400$  mm (diameter $\times$ length)) were adopted. As for the connected long bolts, their specifications were  $\phi 20 \times 5000$  mm and  $\phi 20 \times 3200$  mm in the roof and side walls, separately. The row spacing between anchor bolts on the roof was  $800 \times 900$  mm, while that

on the side walls was  $900 \times 900$  mm. Anchorage lengths on the roof and side walls were 1200 mm and 900 mm, respectively. Plates of anchor bolts on the roof measuring  $\phi 10 \times 150 \times 150$  mm were coordinated with steel ladders. All steel ladders should be lapped to form a whole structure, with a lap-length of 160 mm, (Fig.12).

### 5. Engineering application

Displacement of deep basis points in the roadway in this test was monitored at 188 m, 203 m, 206 m, and 270 m in the intake airway of the 11030 working face in the Zhaogu No.2 coal mine. The layout of the monitoring stations is shown in Fig.13 and the monitoring results are shown in Fig.14.

It can be seen from Fig.14 that roof subsided significantly at a rapid rate in the first 25 days and then subsidence slowly increased after 25 days. At a depth of 8 m from the roof the material rose to about 200 mm during monitoring, while that at a depth of 5 m from the roof increased to about 170 mm. Moreover, displacements at depths of 3 m and 1 m from the roof finally stabilised at about 140 mm and 60 mm. Monitoring results showed that the shallow part of the roof was relatively broken within the depth range extending to 1 m, and there were relatively obvious bedding separations seen at depths of 1 to 3 m, accounting for about 45% of the total deformation. Due to high elongation of the connected long bolts and their ability to provide continuous supporting force, all connected long bolts remained intact: this allowed control over the subsidence of the roof, thus achieving good supporting effect.

## 6. Conclusions

- (1) The transport roadway of the 11050 working face in the No.2[1] coal seam in Zhaogu No.2 coal mine is located in a fold belt where the stress in the surrounding rocks shows characteristics of non-constant pressures caused by stress concentration. Therefore, the plastic zone in the rock surrounding the roadway has a butterfly shape in which the wings are inclined to the roof. The failure of plastic zones in the roof of the roadway is the primary cause of roof caving above the roadway.
- (2) According to the tendency of the failure zone around the roadway to be butterfly - shaped, the method combining connected long bolts and ordinary anchor bolts was adopted for support design and applied in situ. It is found that, due to their high elongation and ability to provide a continuous supporting force, severe deformation of the surrounding rock was controlled and good support effects were obtained.

## 7. References

- [1] Qian Minggao etc. (2003): Mine pressure and rock control [M]. Xuzhou: *China mining university press*.
- [2] Kang Hongpu (2008): The type and interaction of stress field in underground coal mine [J]. *Coal journal*, 12:1329-1335.
- [3] Kang Hongpu, Wang Jinhua, GAO Fuqiang (2009): The stress distribution characteristics of the Surrounding rock and its relationship with the support of the excavation face [J]. *Journal of coal*, (12) : 1585-1593.
- [4] Pu Hai, Miao Xiexing (2004): Numerical simulation of the dynamic distribution of the dynamic distribution of the overburden and surrounding rock of the mining field [J]. *Journal of rock mechanics and engineering*, (07): 1122-1126.
- [5] He Fulian, Liu Liang, Qian Minggao (1995): Analysis and prevention of the roof of the direct top block of loose rock [J]. *Coal*, 04:7-10.
- [6] LI Ji, Ma Nianjie, Zhao Zhiqiang (2017): Butterfly leaf type roof falling mechanism and control technology of mining gateway [J]. *Coal Science and Technology*, 45(12): 46-52.
- [7] Jia Housheng, Ma Nianjie, Zhu Qiankun (2016): Mechanism and control method of roof fall resulted from butterfly plastic zone penetration[J]. *Journal of China Coal Society*, 41(6): 1384-1392.
- [8] Wang Zhiguo, Zhou Hongwei, Xie Heping (2009): Research on fractal characteristics of the network evolution of mining fractures in deep strata [J]. *Geotechnical mechanics*, 30(8): 2403-2408.
- [9] Thomas (1986): Estimation of minimum support resistance and maximum allowable deformation of plastic surrounding rock [J]. *Journal of geotechnical engineering*, 04: 81-88.
- [10] Yu Dongming, Yao Hailin, Lu Zheng, Luo Xingwen (2012): In consideration of the transverse view of the middle principal stress, the plastic solution of the deep buried circular tunneling of the isotropic deep underground [J]. *Journal of geotechnical engineering*, 10: 1850-1857.
- [11] Gou Panfeng, Xin Yajun, Zhang He, Shen Meiyan (2014): The analysis of the characteristics and stability of the anchorage solids in the roof of deep well roadways [J]. *Journal of China mining university*, 05: 712-718.
- [12] He Fulian, Qian Minggao, Shang Duojiang, Zhao Qingbiao, LI Changfu (1994): The mechanism and control of the direct roof fracture in the working face of the fully mechanized mining face [J]. *Journal of China university of mining and technology*, 02: 18-25.
- [13] He Fulian, Liu Liang, Qian Minggao (1995): Analysis and control of the top of the direct top block of loose rock mass [J]. *Coal*, 04: 7-10.
- [14] Dong Fangting, Song Hongwei, Guo Zhihong, Lu Shou-min, Liang Shijie (1994): The theory of loose circle support of surrounding rock of roadway [J]. *Journal of coal*, 01: 21-32.
- [15] Yu Xuefu (1982): The basic rule of axial deformation and the deformation of surrounding rock [J]. *Uranium metallurgy*, 01:8-17+7.
- [16] Guo Xiaofei, Ma Nianjie, Zhao Xidong, et al. (2016): General shapes and criterion for surrounding rock mass plastic zone of round roadway [J]. *Journal of China Coal Society*, 41( 8) :1871-1877.
- [17] Ma Nianjie, LI Ji, Zhao Zhiqiang (2015): Distribution of the deviatoric stress field and plastic zone in circular roadway surrounding rock [J]. *Journal of China mining university*, 44(2): 206-213.
- [18] Chen Guoxiang, Dou Linming, et al. (2008): The Stress Field Distribution in Folding Structure Areas and Its Impaction on Rock Burst [J]. *Journal of rock mechanics and engineering*, 37(6):751-755.
- [19] Liu Hongtao et. al. (2014): Research on lengthening bolt roof support system performance in largely deformed roadway [J]. *Journal of China coal society*, 39(4): 600-607.
- [20] Chang Jucai, Xie Guangxiang (2007): Design on bolt, steelmesh and anchor support parameters for steep inclined seam gateway [J]. *Coal Science and Technology*, 35(01):46-48.